ACS OMEGA

http://pubs.acs.org/journal/acsodf

Article

Synergistic Mechanism of Ultrasonic-Chemical Effects on the CH_4 Adsorption−Desorption and Physicochemical Properties of Jincheng Anthracite

Xiaomin Liang, Tianhe Kang,* Jianting Kang, Haoyang Li, and Wenqing Zhu

Cite This: *ACS Omega* 2023, 8, 1079−1087

Read Online

ACCESS | Metrics & More | Article Recommendations

ABSTRACT: Ultrasonic is a new method to enhance coalbed methane recovery. A deeper comprehension of the synergistic mechanisms of combined ultrasonic-chemical modification on the CH_4 adsorption−desorption capability and physicochemical properties of coal is necessary for potential field implementation, as the modification of coal reservoirs frequently necessitates the addition of chemical reagents. This paper evaluated the CH_4 adsorption−desorption properties of anthracite modified by sodium dodecyl sulfate (SDS) solution, ultrasonic modification, and combined ultrasonic-SDS modification. Fourier transform infrared spectroscopy, low-temperature nitrogen adsorption, and micro-CT were applied to elucidate the synergistic mechanism of the combined modification. The research results show that the SDS solution reduces the saturated adsorption capacity of anthracite and increases its final desorption rate by dissolving clay minerals and the physical adsorption masking effect of SDS micelles on the coal surface. Some surface groups with low bond energy are broken or evaporated under mechanical vibration and thermal effects generated by ultrasonic. The original fractures are expanded and connected, which changes the adsorption−desorption properties of anthracite. The synergistic effect of the combined modification of ultrasonic-SDS can promote the penetration range and chemical reaction efficiency of the SDS solution, which expands the effective range of ultrasonic. After combined modification, the amount of aromatics, oxygen-containing functional groups, and aliphatic hydrocarbons on the surface of coal is reduced. The connected porosity of coal samples accounts for 91.5% of the total porosity. As a result, the saturated adsorption capacity of anthracite reduces by 26.7%, and the final desorption rate increases by 28.0%. The effect of the combined ultrasonic-chemical modification is better than that of a single modification.

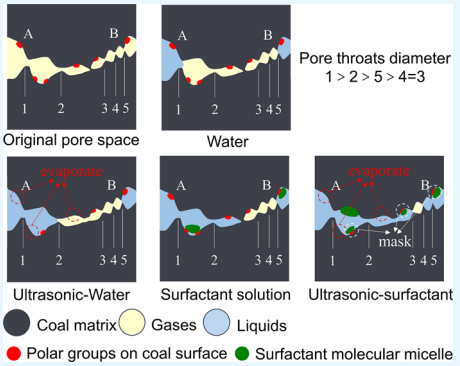

1. INTRODUCTION

Coalbed methane (CBM) is a clean energy source associated with coal, with 90% of its reserves adsorbed on the surface of the coal matrix.[1] China is the third-largest CBM resource country after Australia and the United States. The low permeability and high adsorption of Chinese CBM reservoirs, however, have resulted in a current utilization rate of less than 1%, an engineering success rate of less than 60%, and a capacity conversion rate of less than 50%, indicating a mismatch between CBM production and resources.[2]

For low permeability and high adsorption CBM reservoirs, modification is required.[3] The first category is the single modification methods. Examples include hydraulic fracturing,[4] high-energy gas fracturing,[5] gas injection drive technology,[6,7] chemical stimulation,[8] acoustic field,[9] electric field,[10] and microwave field stimulation.[11] However, there are drawbacks to the single modification approach, such as the fact that the chemical solution can only dissolve a portion of the mineral and that the pore-throat capillary force restricts the penetration range. The second category is combination modification methods. Such as using a composite fracturing fluid with surfactants and acid reagents to increase the range of permeation,[12,13] a synergistic effect of hydraulic fracturing-ultrasonic excitation to increase reservoir seepage, and electrochemical treatment to increase methane desorption and seepage in coalbed.[14]

Since the 1950s, ultrasonic technology has been widely used in oil extraction.[15] According to experiments, the combined use of ultrasonic and chemical reagents restores 49% of the permeability in blocked cores.[16] Ultrasonic can lower the viscosity of crude oil, reduce the capillary forces in pores,[17] change the pore structure, and accelerate the chemical reaction rate to enhance oil recovery. Using ultrasonic or combined

Received: October 4, 2022
Accepted: November 23, 2022
Published: December 21, 2022

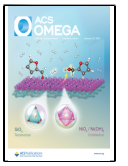

https://doi.org/10.1021/acsomega.2c06425
ACS Omega 2023, 8, 1079−1087

ultrasonic-chemical methods for reservoir physical modification is considered one of the most promising modern techniques.[18]

Ultrasonic is also extensively studied for enhance coalbed methane recovery.[19] The pores in coal seams develop, expand, and connect under the mechanical vibration, thermal, and cavitation effects generated by ultrasonic.[20] This positively impacts gas transport in the CBM production process by reducing the methane adsorption area and encouraging the desorption and diffusion of CH_4 within the coal matrix.[21,22] Although some good results have been obtained from the existing studies,[23] the mechanism of the synergistic effect of the combined ultrasonic-chemical modification on the CH_4 adsorption−desorption properties has not been reported. An anionic surfactant can affect the CH_4 adsorption−desorption properties by altering the distribution of coal surface groups.[24] It was widely used in unconventional gas extraction as a key component of fracturing fluid chemistry.[25,26] Therefore, it is essential to fully understand the synergistic mechanism of the combined ultrasonic-surfactant modification on the CH_4 adsorption−desorption properties of coal for the field application of ultrasonic technology.

This paper studied the CH_4 adsorption−desorption properties of anthracite samples before and after sodium dodecyl sulfate (SDS) solution modification, ultrasonic modification, and combined ultrasonic-SDS modification. The surface groups and pore characteristics were analyzed to explain the synergistic mechanism of combined ultrasonic-chemical modification.

2. RESULTS AND DISCUSSION

2.1. Influence on the CH_4 Adsorption−Desorption Properties in Anthracite. Figure 1 shows the capacity of

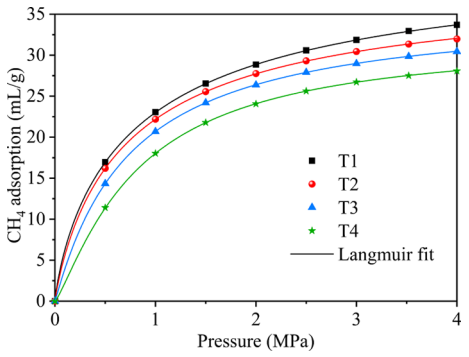

Figure 1. Effect of CH_4 adsorption with pressure before and after modification.

CH_4 adsorption by the anthracite samples before and after modification at different adsorption pressures. Table 1 shows the Langmuir fitted parameters and the final desorption rate of the test.

The Langmuir isothermal adsorption equation was used to calculate the CH_4 adsorption on anthracite samples.[14]

$$V = \frac{V_L P}{P_L + P} \tag{1}$$

where V is the amount of adsorbed gas (mL/g); P is the gas equilibrium pressure (MPa); V_L is the maximum amount of adsorbed gas; and P_L is the gas equilibrium pressure of half of the saturated adsorption amount V_L (MPa). V_L and P_L are Langmuir constants.

Table 1. Results of the Langmuir Fit and the Final Desorption Rate

samples	V_L (mL/g)	P_L (MPa)	correlation coefficient R^2	final desorption rate (%)
T1	43.11	1.24	0.998	72.4
T2	39.13	1.30	0.999	79.9
T3	36.58	1.38	0.999	83.5
T4	31.61	1.41	0.998	92.7

$V_L = a$, $1/P_L = b$, eq 1 can be expressed as

$$V = \frac{abP}{1 + bP} \tag{2}$$

Equation 2 was used to fit the scatterplot of various adsorption equilibrium pressure points and the corresponding amounts of adsorption to obtain the adsorption parameters.

The final desorption rate is the ratio of the amount of methane desorption to the amount of methane adsorption at equilibrium. The higher final desorption rate means that methane is more easily converted from an adsorbed state to a free state. When the adsorption pressure increases to 4 MPa and the adsorption equilibrium is reached, the adsorption tank pressure is reduced to atmospheric pressure and the desorption process begins. The desorption amount at different time intervals was recorded manually. When the desorption rate was less than 0.1 mL/min, the desorption process was finished. The final desorption rate equation is as follows

$$\eta = \frac{V_0}{V} \times 100\% \tag{3}$$

where η is the final desorption rate (%); V is the adsorption amount of the anthracite samples to reach the adsorption equilibrium (mL/g); and V_0 is the amount of CH_4 desorption (mL/g).

The Langmuir constants are important indicators of the sorption capacity of coal, with larger V_L and minor P_L indicating stronger adsorption capacity. The R^2 of the adsorption results from the Langmuir equation fits all exceeded 0.99, which was in accordance with the Langmuir model.

According to Figure 1 and Table 1, the amount of CH_4 adsorbed on anthracite is proportional to the adsorption pressure. The saturated adsorption capacity of the raw samples was 43.11 mL/g. Compared with T1, the saturated adsorption capacity of T2, T3, and T4 decreased to 39.13, 36.56, and 31.61 mL/g, which were reduced by 9.2, 15.2, and 26.7%, respectively.

Table 1 shows that the final desorption rate for the raw samples was 72.4%, implying that CH_4 is not easily desorbed from the coal. The final desorption rates of T2, T3, and T4 were 79.9, 83.5, and 89.7%, respectively, which were increased by 10.3, 15.4, and 28.0% compared with T1.

The experiments showed that the ultrasonic was more effective than the SDS solution in altering the CH_4 adsorption−desorption properties of coal, and the combined ultrasonic-SDS modification was more effective than the single modification. The synergistic mechanism of the combined ultrasonic-SDS modification would be analyzed by the changes in surface groups and pore characteristics in anthracite.

2.2. Analysis of Surface Groups Based on FTIR. The surface groups are atoms or groups at the edges of the basic

https://doi.org/10.1021/acsomega.2c06425
ACS Omega 2023, 8, 1079−1087

units of the coal chemical structure. They are one of the critical factors that dominate the adsorption properties of coal.[27] Figure 2 shows the infrared spectrums of the anthracite samples before and after modification.

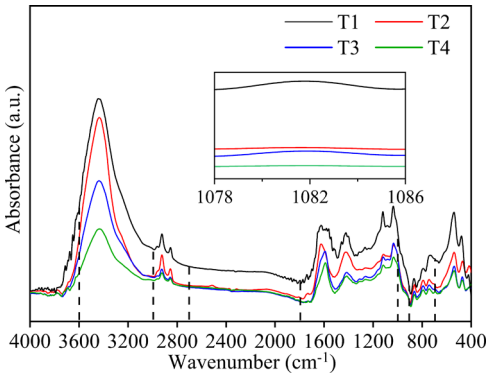

Figure 2. Infrared spectrums of the anthracite samples before and after modification.

As can be seen from Figure 2, the distribution pattern of the infrared spectrums was approximately the same for the different samples. However, the intensity and area of the absorption peaks have considerable differences. The characteristic peaks of significant changes in coal are at 3600−3000 cm^{-1} (−OH), 3000−2700 cm^{-1} ($-CH_3$ and $-CH_2$), 1800−1000 cm^{-1} (oxygen-containing functional groups), and 900−700 cm^{-1} (aromatic ring structures).[28]

(1) The T2 infrared spectrum showed that the characteristic peak areas of hydroxyl groups, oxygen-containing functional groups, and aromatic rings decreased gradually. As shown in Figure 3, the polar hydrophilic

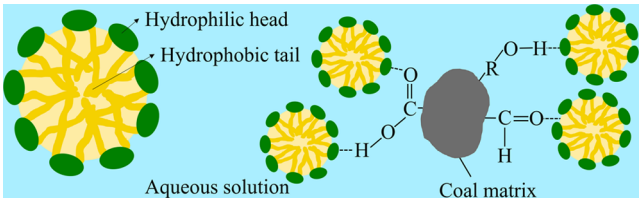

Figure 3. Schematic diagram of the masking effect of SDS micelles on polar groups.

groups on the surface of SDS micelles physically adsorb onto the polar oxygen-containing functional groups on the anthracite surface through van der Waals forces, masking some of the oxygen-containing functional groups and impeding the out-of-plane deformation vibrations of the aromatic hydrocarbons.[29] Also worth mentioning is that the decline in peak intensity at 1082 cm^{-1} suggests a decline in smectite minerals.[30] Due to their smaller mesoporous structure than anthracite, clay minerals are easier to adsorb methane. As a result, reducing clay minerals in coal will diminish the methane adsorption site, decreasing the methane adsorption capacity of anthracite.[31]

(2) The T3 infrared spectrum showed that ultrasonic was more effective than SDS solution in changing the surface groups of the anthracite. Some oxygen-containing functional groups with low bond energy, most aliphatic molecules, and some aromatic rings in anthracite macromolecules are broken or evaporated by the mechanical vibrations and thermal effects generated by ultrasonic. Figure 4 shows the schematic diagram of the changes in the molecular structure of coal by ultrasonic.[32]

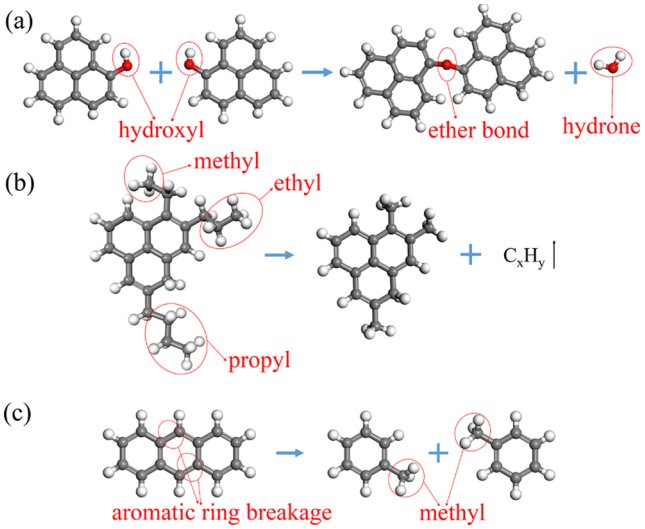

Figure 4. Schematic diagram of the coal molecular structure change by ultrasonic: (a) hydroxyl removal, (b) alkane side chains are broken, and (c) aromatic ring breakage.

(3) The degree of change in the area of the characteristic peaks in the T4 infrared spectrum is significantly higher than that in the other samples. Ultrasonic loading directly affects the surface group distribution pattern of coal and makes the SDS micelles more easily adsorbed on the anthracite surface.[33]

Studies have shown that the CH_4 adsorption capacity of coal is proportional to the content of aromatic groups.[34] The adsorption heat generated by the adsorption of CH_4 on coal is proportional to the content of oxygen-containing functional groups in its molecular structure.[35] The number of methyl and methylenes is proportional to the adsorption potential well of coal for CH_4.[36] Thus, the reduction in the number of aromatic groups, oxygen-containing functional groups, and aliphatic hydrocarbons in coal contributes to weakening of the CH_4 adsorption capacity.

2.3. Analysis of Nano-Scale Pore Characteristics Based on LTNA. The pore characteristics of coal are key to its CH_4 adsorption−desorption properties. The amount of CH_4 adsorbed in coal is proportional to the surface area. The larger the average pore diameter and pore volume of coal, the easier the desorption of CH_4. The experimental data were analyzed using the International Union of Pure and Applied Chemistry (IUPAC) classification scheme for coal pores (micropores <2 nm; mesopores 2−50 nm; macropores >50 nm).

Table 2 and Figure 5 show the pore characteristics of the anthracite samples before and after modification. The results showed that the average pore diameter and pore volume of the modified coal samples increased, but the specific surface area decreased. This is one of the reasons for the decrease in the saturated adsorption capacity and the increase in the final desorption rate of the modified coal samples.

https://doi.org/10.1021/acsomega.2c06425
ACS Omega 2023, 8, 1079−1087

Table 2. Pore Characteristics of the Anthracite before and after Modification

samples	average pore diameter (nm)	pore volume (cm^3/g)	specific surface area (m^2/g)
T1	2.6712	0.003964	4.7553
T2	2.7493	0.004676	4.1145
T3	4.3688	0.007341	3.8429
T4	4.7148	0.008319	2.7359

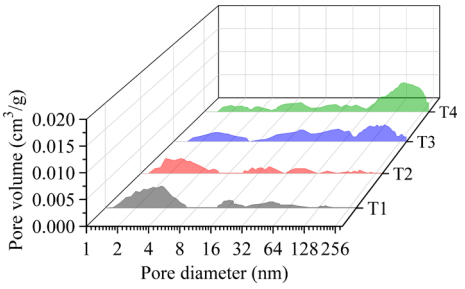

Figure 5. Results of change in pore volume of the anthracite before and after modification.

(1) Compared with T1, the specific surface area of T2 was reduced by 13.5%. The pore volume of the mesopores and macropores of T2 varied less when modified with the SDS solution. However, the micropore volume of T2 is reduced. Combined with Figure 2, it is the result of the leaching of smectite minerals from the coal by the SDS solution.

(2) T3 has a larger volume of mesopores and macropores than T1, a smaller volume of micropores than T1, and the specific surface area decreased by 19.2%. With ultrasonic loading, the micropores and mesopores of T3 were extended to macropores and mesopores.

(3) The specific surface area decreased by 42.5% compared to T1, while the volume of the micropores decreased significantly, and the mesopores and macropores increased. The smaller micropores in T4 are enlarged to mesopores and macropores by the combined ultrasonic-SDS modification.

2.4. Analysis of Micro-Scale Pore Characteristics Based on Micro-CT. The 3D reconstruction results of micro-CT experiments provide non-destructive quantitative analysis and visualization of the micro-scale pore structure of coal samples and quantitative analysis of the mineral content.[37] The 3D-REV is a small cube that can reflect the pore structure of the whole coal sample. When the side length was greater than 280 voxels, the porosity of coal tended to be a certain value and was approximately equal to the porosity of the whole sample.[38] In this study, a cube with a side length of 500 voxels (9.8 mm) is extracted as 3D-REV from the CT scan digital core before and after modification.

Figure 6 shows the total porosity, connected porosity, and mineral fraction of the 3D-REV before and after modification. Figure 7 shows the visual changes in the coal structure of 3D-REV before and after modification. The sites selected by the black lines in these figures exemplify a typical change in the coal structure. The CH_4 adsorption capacity of anthracite is inversely proportional to its total porosity. The larger the proportion of connected porosity to the total porosity, the easier the methane desorption and seepage from coal.

Figure 6a demonstrates that after modification, the total porosity of T2 increased from 1.5 to 2.2%, T3 from 1.7 to 3.1%, and T4 from 1.2 to 4.2%, respectively, increasing by 41.2, 83.2, and 249.0%. As shown in Figure 6b, the connected porosity after T4 modification accounted for 91.5% of the total porosity, 67.9% of T3, and 44.9% of T2. Figure 6c shows that after modification of T2, T3, and T4, the mineral fraction decreases from 3.1, 1.8, and 2.7 to 2.4, 1.8, and 1.1%, respectively. The mineral removal rates of T2, T3, and T4 were 22.1, 2.7, and 59.4%, respectively.

This phenomenon indicates that removing minerals is the main reason for new fractures after T2 modification. The blue mineral band before modification (Figure 7a) vanished after T2 modification to form new fractures (Figure 7d). Ultrasonic loading leads to the expansion and connection of the original fractures mainly through mechanical vibration and cavitation effects, with less effect on the mineral content of the coal, as shown in Figure 7b,e. The removal of the blue mineral in Figure 7c resulted in the connection of the original fracture extension in Figure 7f, indicating that the removal of the mineral facilitated the increase in porosity and pore connectivity of the coal sample.

The 3D-REV was divided into 500 layers along the *Z*-axis direction. The total porosity, connected porosity, and mineral fraction were calculated for each *XY* interface to accurately analyze the effect of different modifications on the coal samples, as shown in Figure 8.

The removal of minerals in T2 mainly occurs in the fracture-connected area, as shown in Figure 8a,b, near 150 voxels. At the same time, it can be found that removing some minerals will lead to an increase in the total porosity and connected porosity, such as around 250 and 385 voxels.

Figure 8d shows that T3 has little effect on mineral fraction. In Figure 8c, the porosity of 100−400 voxels is increased by

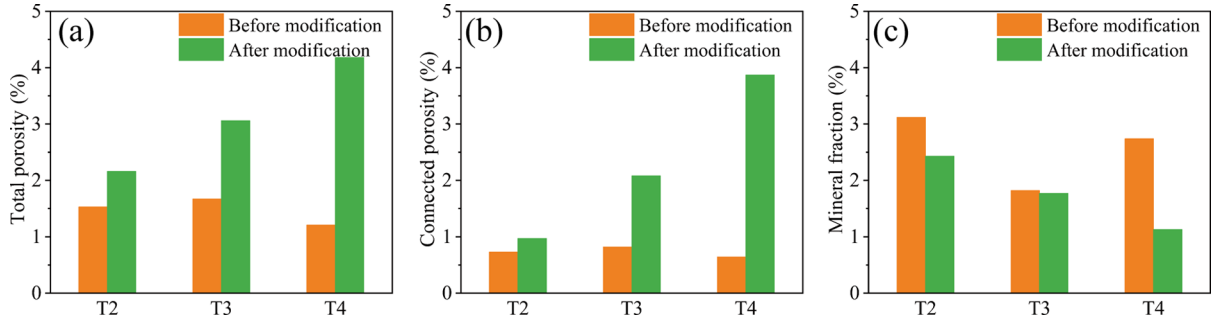

Figure 6. Porosity and mineral fraction of the 3D-REV before and after modification. (a) Total porosity; (b) connected porosity; and (c) mineral fraction.

https://doi.org/10.1021/acsomega.2c06425
ACS Omega 2023, 8, 1079−1087

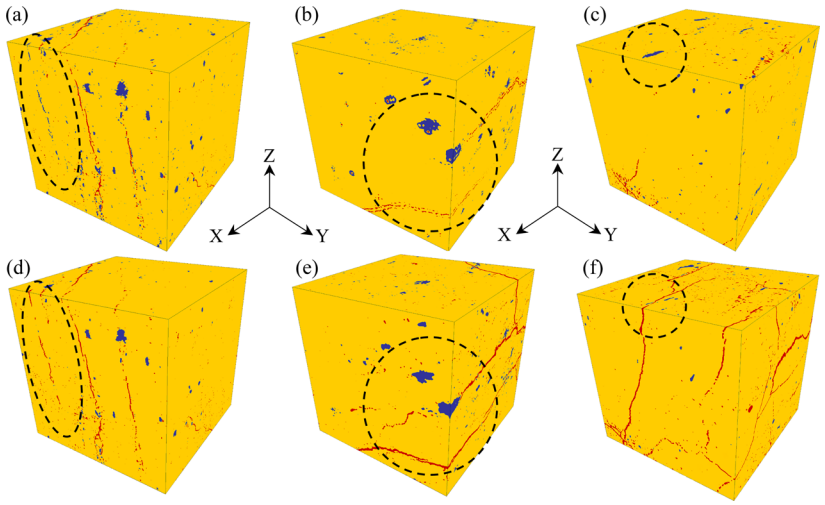

Figure 7. 3D-REV of coal samples before and after modification. (a,d) Before and after T2 modification; (b,e) before and after T3 modification; and (c,f) before and after T4 modification. The yellow, blue, and red zones represent the coal matrix, the minerals, and the pores/fractures, respectively.

fracture extension and connection in the range 0−100 voxels and 400−500 voxels, indicating that T3 mainly improves the porosity by extending and connecting the original fractures.

It can be seen in Figure 8e that the total porosity and connected porosity of T4 before modification are uniformly distributed along the *Z*-axis. After modification, the mineral fraction of T4 decreases uniformly, as shown in Figure 8f. However, the total porosity and connected porosity of the modified 0−250 voxels is much higher than that of the 250−500 voxels. This result indicates that ultrasonic and SDS solutions have a synergistic effect at 0−250 voxels, resulting in the formation of many new pores.

2.5. Discussion of Synergistic Mechanisms. Surfactant solutions can dissolve part of the clay minerals, adsorb and mask to change the distribution pattern of surface groups on the coal, and reduce the capillary forces in the pores by reducing the interfacial tension between coal and water accessible for liquids to enter the smaller pores.[39]

Coal, as a solid medium, produces mechanical vibrations and thermal effects under the action of ultrasonic. The liquid within coal will be a prerequisite for ultrasonic cavitations to occur. When ultrasonic is applied to the coal liquid, the microbubbles in the liquid are continuously compressed, expanded, and oscillated until they explode. The burst of the micro-air bubbles results in a temperature and pressure of about 5000 K and 50 MPa, as well as powerful shock waves and microjets traveling at 110 m/s.[40] The thermal, mechanical vibration, and cavitation effects produced by ultrasonic change the surface groups and pore characteristics of coal, producing the "sonocapillary effect", which will effectively enhance the penetration depth of liquid in capillaries.[41]

The coupling of SDS solution and ultrasonic during the combined ultrasonic-chemical modification significantly changes the surface groups and pore structure of coal. The combined ultrasonic-chemical modification increases the depth of penetration of the chemical solution into the coal matrix, improving the efficiency of chemical reactions and expanding the coverage of liquid media for ultrasonic propagation. In other words, the synergistic effect of combined ultrasonic-chemical modification not only enhances the reaction efficiency of the chemical solution but also helps to increase the effective range of ultrasonic. The two promote each other to improve the degree of change in the physicochemical properties of coal and make CBM desorption easier.

3. CONCLUSIONS

This paper investigates the synergistic mechanism of combined ultrasonic-chemical modification in coal reservoirs. The aim is to understand further the implication of the interaction between coal and surfactant on CH_4 production during ultrasonic action. The main results can be summarized as follows:

(1) Both surfactant and ultrasonic modification change the CH_4 adsorption−desorption properties of coal samples. Compared with water−coal samples, the surfactant modification, ultrasonic modification, and combined ultrasonic-surfactant modification reduce the saturated adsorption capacity by 9.2, 15.2, and 26.7% and increase the final desorption rate by 10.3, 15.4, and 28.0%, respectively. The ultrasonic modification is better than the surfactant modification, and the effect of the combined ultrasonic-surfactant modification is better than that of a single method.

(2) The surfactant solution mainly improves the porosity by removing minerals in the fracture and changes the distribution of surface groups on the coal by physical adsorption of molecular micelles. The ultrasonic increases the porosity by expanding and connecting the original fractures and changes the distribution pattern of coal surface groups by mechanical vibration and thermal effect.

(3) Illuminates the synergistic mechanism of the combined ultrasonic-chemical modification: ultrasonic through vibration, heat, and "sonocapillary effect" not only promotes the efficiency of a chemical reaction but also expands the effective range of ultrasonic propagation by increasing the penetration depth of chemical solution in the coal matrix. The two promote each other and improve the degree of change in the physicochemical properties of coal.

(4) The synergistic mechanism of the combined ultrasonic-chemical modification on the CH_4 adsorption−desorp-

https://doi.org/10.1021/acsomega.2c06425
ACS Omega 2023, 8, 1079−1087

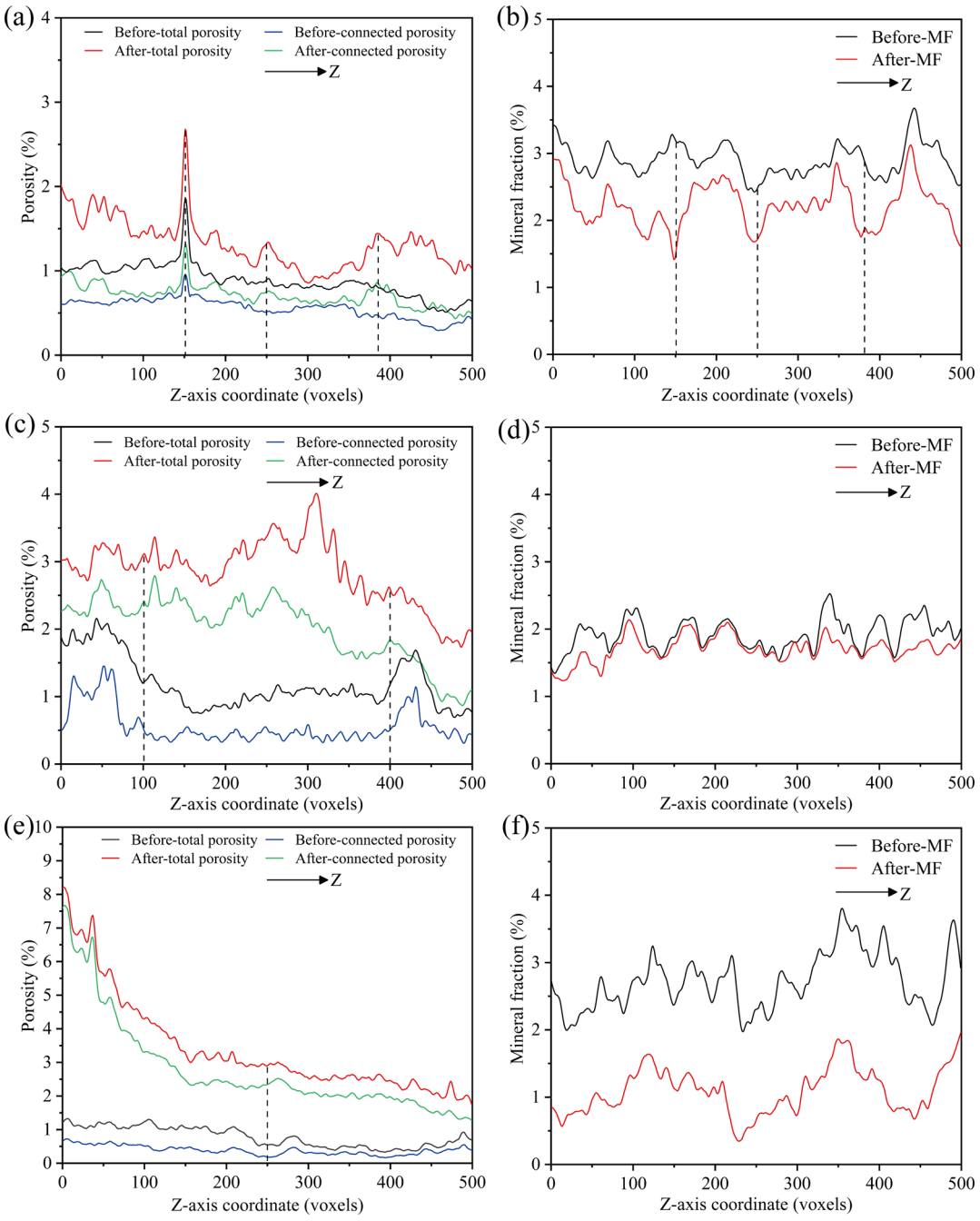

Figure 8. Porosity distribution and mineral fraction of the 3D-REV along the *Z*-axis before and after modification. (a,b) T2 sample; (c,d) T3 sample; and (e,f) T4 sample.

tion properties of coal is elucidated, which can provide a theoretical basis for the field application of ultrasonic technology.

4. EXPERIMENTAL SECTION

4.1. Materials. The anthracite samples used for the experiments were taken from the Sihe Mine, Jincheng City, Shanxi Province, China. Table 3 shows the basic information of Jincheng anthracite.

SDS is a typical anionic surfactant with the molecular formula: $C_{12}H_{25}SO_3Na$. The surface tension of surfactant solution reaches the minimum value when it is higher than the critical micelle concentration (CMC). The CMC of SDS solution at 298 K was 0.009 mol/L. In order to increase the effectiveness of the chemical modification experiments on the anthracite samples, the SDS solution with a concentration of 0.02 mol/L was used.[42]

Table 3. Basic Information of Jincheng Anthracite[a]

		proximate analysis (wt %)		
samples	$R_{o,max}$ (%)	moisture, ad	ash yield, ad	volatile matter, daf
anthracite	2.86	1.65	5.21	6.12

[a]ad: air dried basis; daf: dry ash-free basis.

4.2. Experimental Apparatus. Figure 9 shows the schematic of the ultrasonic experimental device, which mainly consists of the ultrasonic wave generator, ultrasonic transducer,

https://doi.org/10.1021/acsomega.2c06425
ACS Omega 2023, 8, 1079−1087

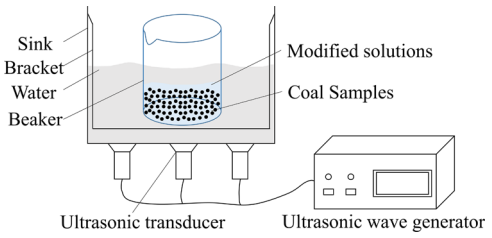

Figure 9. Schematic of the ultrasonic modification experimental device.

sink, bracket, beaker, modified solutions, and coal samples. Ningbo Kemai Instruments Factory supplied the SKE-6S ultrasonic generator, the ultrasonic frequency was 40 kHz, and the ultrasonic power was 180 W.

In this device, the ultrasonic transducer placed at the bottom of the sink converts the high-frequency alternating current generated by the ultrasonic generator into high-frequency mechanical vibration, creating an upward-propagating ultrasonic field in the water of the sink and further acting on the coal samples in the beaker.

4.3. Experimental Process. The anthracite samples were milled and sieved for adsorption−desorption property tests (0.18−0.25 mm diameter), low-temperature nitrogen adsorption (LTNA) tests (0.18−0.25 mm diameter), and Fourier transform infrared (FTIR) tests (<74 μm). Cylindrical samples with a diameter of 20 mm and a height of 30 mm were cored in a direction perpendicular to the laminae of the anthracite samples and used for CT scanning.

Table 4 shows the experimental programs. Before modification, the anthracite samples were dried in a vacuum oven at

Table 4. Experimental Programs

samples	modified solutions	concentration (mol/L)	ultrasonic frequency (kHz)	ultrasonic power (W)
T1	H_2O			
T2	SDS	0.02		
T3	H_2O		40	180
T4	SDS	0.02	40	180

378 K according to GB/T 19560-2008 until a constant weight was achieved. T1 and T2 were soaked for 120 h. T3 and T4 were soaked for 120 h and then transferred to the ultrasonic modification experimental device for 30 min. After modification, the coal samples were dried again.

The CH_4 adsorption capacity of anthracite samples was obtained from the 3H-2000PHD high-pressure gas adsorption and desorption rate analyzer produced by BeiShiDe Instrument Technology. The coal adsorption test was carried out by setting the maximum adsorption pressure to 4 MPa with a total of eight adsorption equilibrium pressure points. During the test, the anthracite samples were vacuum-degassed first, the degassing temperature was 378 K, and the degassing time was 300 min. After degassing, the anthracite samples were kept at 313 K for 120 min, and gas adsorption was started after degassing was completed. The mean pressure difference method is adopted for adsorption. When the methane in the reference chamber reaches the current pressure equilibrium, it will be automatically pressurized to the next adsorption equilibrium pressure point, and the adsorption will be completed when it reaches 4 MPa. The adsorption equilibrium time was 4 h, and the equilibrium standard deviation was 0.008 MPa. The gas desorption properties of the anthracite samples were tested by 3H-2000PHD as described above.

FTIR techniques can obtain the surface group distribution of anthracite samples. The dried anthracite samples were mixed and tableted with potassium bromide (KBr) at 1:150 wt %. The test of the surface groups was conducted by the Nicolet iS5 FTIR instrument produced by the Thermo Fisher company. The detection spectral range of the instrument was 7800−350 cm^{-1}. The resolution and accuracy of the instrument were better than 0.5 and 0.01 cm^{-1}, respectively, and the signal-to-noise ratio was 40,000:1.

LTNA is a commonly used method for measuring the structural and distributional characteristics of coal pores in the range of 1.7 to 300 nm. The average pore diameter, pore volume, and specific surface area of the anthracite samples can be analyzed by the ASAP2020HD88 nitrogen adsorption−desorption apparatus from Micromeritics company.

Micro-CT is a method for non-destructive analysis of the structure, morphology, and connectivity of micropores in coal. The micro-CT scanning of the anthracite samples was conducted with a nanoVoxel-4000 open tube reflective high penetration CT system produced by Sanying Precision Instruments Co., Ltd. The scanning voltage was 200 kV, the scanning current was 160 μA, the exposure time was 3.0 s, and the spatial resolution was 10.34 μm. After scanning and processing the entire sample before and after modification, 16 bit images with 2100 × 2100 × 3072 voxels were obtained.

AUTHOR INFORMATION

Corresponding Author

Tianhe Kang − *Key Laboratory of In-situ Property Improving Mining of Ministry of Education, Taiyuan University of Technology, Taiyuan 030024, People's Republic of China;* orcid.org/0000-0002-1767-6168; Email: kangtainhe@126.com

Authors

Xiaomin Liang − *Key Laboratory of In-situ Property Improving Mining of Ministry of Education, Taiyuan University of Technology, Taiyuan 030024, People's Republic of China*

Jianting Kang − *College of Safety and Emergency Management Engineering, Taiyuan University of Technology, Taiyuan 030024, People's Republic of China*

Haoyang Li − *Key Laboratory of In-situ Property Improving Mining of Ministry of Education, Taiyuan University of Technology, Taiyuan 030024, People's Republic of China*

Wenqing Zhu − *Key Laboratory of In-situ Property Improving Mining of Ministry of Education, Taiyuan University of Technology, Taiyuan 030024, People's Republic of China*

Complete contact information is available at: https://pubs.acs.org/10.1021/acsomega.2c06425

Notes

The authors declare no competing financial interest.

ACKNOWLEDGMENTS

This research was supported financially by the National Natural Science Foundation of China (41902179, 42072203, and U1810102).

https://doi.org/10.1021/acsomega.2c06425
ACS Omega 2023, 8, 1079−1087

REFERENCES

(1) Zhao, L.; Guanhua, N.; Lulu, S.; Qian, S.; Shang, L.; Kai, D.; Jingna, X.; Gang, W. Effect of ionic liquid treatment on pore structure and fractal characteristics of low rank coal. *Fuel* **2020**, *262*, 116513.

(2) Wang, Z.; Wang, X. Promotion effects of microwave heating on coalbed methane desorption compared with conductive heating. *Sci. Rep.* **2021**, *11*, 1−16.

(3) Li, H.; Xu, C.; Ni, G.; Lu, J.; Lu, Y.; Shi, S.; Li, M.; Ye, Q. Spectroscopic (FTIR, 1H NMR) and SEM investigation of physicochemical structure changes of coal subjected to microwave-assisted oxidant stimulation. *Fuel* **2022**, *317*, 123473.

(4) Liu, Y.; Tang, D.; Xu, H.; Zhao, T.; Hou, W. Effect of interlayer mechanical properties on initiation and propagation of hydraulic fracturing in laminated coal reservoirs. *J. Pet. Sci. Eng.* **2022**, *208*, 109381.

(5) Chu, H.; Yang, X.; Wang, C.; Liang, W. Study on the coal damage and fracture mechanism under multiple actions of blasting stress wave. *Arabian J. Sci. Eng.* **2021**, *46*, 10847−10854.

(6) Liang, W.; Yan, J.; Zhang, B.; Hou, D. Review on coal bed methane recovery theory and technology: Recent progress and perspectives. *Energy Fuels* **2021**, *35*, 4633−4643.

(7) Luo, C.; Zhang, D.; Lun, Z.; Zhao, C.; Wang, H.; Pan, Z.; Li, Y.; Zhang, J.; Jia, S. Displacement behaviors of adsorbed coalbed methane on coals by injection of SO2/CO2 binary mixture. *Fuel* **2019**, *247*, 356−367.

(8) Smith, H. J.; Schweitzer, H.; Barnhart, E.; Orem, W.; Gerlach, R.; Fields, M. W. Effect of an algal amendment on the microbial conversion of coal to methane at different sulfate concentrations from the Powder River Basin, USA. *Int. J. Coal Geol.* **2021**, *248*, 103860.

(9) Jiang, Y.; Song, X.; Liu, H.; Cui, Y. Laboratory measurements of methane desorption on coal during acoustic stimulation. *Int. J. Rock Mech. Min. Sci.* **2015**, *78*, 10−18.

(10) Guo, H.; Chen, C.; Liang, W.; Zhang, Y.; Duan, K.; Zhang, P. Enhanced biomethane production from anthracite by application of an electric field. *Int. J. Coal Geol.* **2020**, *219*, 103393.

(11) Huang, J.; Xu, G.; Liang, Y.; Hu, G.; Chang, P. Improving coal permeability using microwave heating technology—A review. *Fuel* **2020**, *266*, 117022.

(12) Zepeng, W.; Zhaolong, G.; Ruihui, L.; Xianfeng, L.; Haoming, W.; Shihui, G. Effects of acid-based fracturing fluids with variable hydrochloric acid contents on the microstructure of bituminous coal: An experimental study. *Energy* **2022**, *244*, 122621.

(13) Wang, Z.; Liu, S.; Qin, Y. Coal wettability in coalbed methane production: A critical review. *Fuel* **2021**, *303*, 121277.

(14) Guo, J.; Kang, T.; Kang, J.; Chai, Z.; Zhao, G. Accelerating methane desorption in lump anthracite modified by electrochemical treatment. *Int. J. Coal Geol.* **2014**, *131*, 392−399.

(15) Wang, Z.; Fang, R.; Guo, H. Advances in ultrasonic production units for enhanced oil recovery in China. *Ultrason. Sonochem.* **2020**, *60*, 104791.

(16) Wang, Z.; Xu, Y.; Bajracharya, S. The comparison of removing plug by ultrasonic wave, chemical deplugging agent and ultrasound−chemical combination deplugging for near-well ultrasonic processing technology. *Ultrason. Sonochem.* **2015**, *27*, 339−344.

(17) Alhomadhi, E.; Amro, M.; Almobarky, M. Experimental application of ultrasound waves to improved oil recovery during waterflooding. *J. King Saud Univ. Sci.* **2014**, *26*, 103−110.

(18) Abramov, V. O.; Mullakaev, M. S.; Abramova, A. V.; Esipov, I. B.; Mason, T. J. Ultrasonic technology for enhanced oil recovery from failing oil wells and the equipment for its implemention. *Ultrason. Sonochem.* **2013**, *20*, 1289−1295.

(19) Liu, P.; Liu, A.; Zhong, F.; Jiang, Y.; Li, J. Pore/fracture structure and gas permeability alterations induced by ultrasound treatment in coal and its application to enhanced coalbed methane recovery. *J. Pet. Sci. Eng.* **2021**, *205*, 108862.

(20) Liu, P.; Fan, L.; Fan, J.; Zhong, F. Effect of water content on the induced alteration of pore morphology and gas sorption/diffusion kinetics in coal with ultrasound treatment. *Fuel* **2021**, *306*, 121752.

(21) Liu, P.; Liu, A.; Liu, S.; Qi, L. Experimental evaluation of ultrasound treatment induced pore structure and gas desorption behavior alterations of coal. *Fuel* **2022**, *307*, 121855.

(22) Shi, Q.; Qin, Y.; Li, J.; Wang, Z.; Zhang, M.; Song, X. Simulation of the crack development in coal without confining stress under ultrasonic wave treatment. *Fuel* **2017**, *205*, 222−231.

(23) Liu, P.; Fan, L.; Li, Q.; Zhong, F. Power ultrasound assisted coalbed methane enhancement recovery: Field application and performance evaluation in underground coal mine. *Fuel* **2022**, *324*, 124575.

(24) Abdulelah, H.; Mahmood, S. M.; Al-Mutarreb, A. Effect of Anionic Surfactant on Wettability of Shale and Its Implication on Gas Adsorption/Desorption Behavior. *Energy Fuels* **2018**, *32*, 1423−1432.

(25) Shibaev, A. V.; Osiptsov, A. A.; Philippova, O. E. Novel trends in the development of surfactant-based hydraulic fracturing fluids: a review. *Gels* **2021**, *7*, 258.

(26) Guanhua, N.; Hongchao, X.; Shang, L.; Qian, S.; Dongmei, H.; Yanying, C.; Ning, W. The effect of anionic surfactant (SDS) on pore-fracture evolution of acidified coal and its significance for coalbed methane extraction. *Adv. Powder Technol.* **2019**, *30*, 940−951.

(27) Patricia, O.; Blandón, A.; Perea, C.; Mastalerz, M. Petrographic characterization, variations in chemistry, and paleoenvironmental interpretation of Colombian coals. *Int. J. Coal Geol.* **2020**, *227*, 103516.

(28) Xu, Q.; Liu, R.; Yang, H. Effect of acid and alkali solutions on micro-components of coal. *J. Mol. Liq.* **2021**, *329*, 115518.

(29) Zhang, H.; Xi, P.; Zhuo, Q.; Liu, W. Construction of molecular model and adsorption of collectors on bulianta coal. *Molecules* **2020**, *25*, 4030.

(30) Zhang, X.; Zhang, R.; Kang, T.; Hu, Y. The adsorption and desorption behavior of CH4 on Jincheng anthracite modified in Fe3+ and Cu2+ ion electrolytes. *Energy Fuels* **2020**, *34*, 1251−1258.

(31) Feng, Z. C.; Cai, T. T.; Zhou, D.; Zhao, D.; Zhao, Y. S.; Wang, C. Temperature and deformation changes in anthracite coal after methane adsorption. *Fuel* **2017**, *192*, 27−34.

(32) Zhang, L.; Kang, T.; Kang, J.; Zhang, X.; Zhang, B.; Guo, J.; Chai, Z. Response of Molecular Structures and Methane Adsorption Behaviors in Coals Subjected to Cyclical Microwave Exposure. *ACS omega* **2021**, *6*, 31566−31577.

(33) Yang, L.; Li, X.; Li, W.; Yan, X.; Zhang, H. Intensification of interfacial adsorption of dodecylamine onto quartz by ultrasonic method. *Sep. Purif. Technol.* **2019**, *227*, 115701.

(34) Zhang, H.; Lun, Z.; Zhou, X.; Wang, H.; Zhao, C.; Zhang, D. Role of H_2O of Gas-Bearing Shale in Its Physicochemical Properties and CH_4 Adsorption Performance Alteration Due to Microwave Irradiation. *Energy Fuels* **2021**, *35*, 19464−19480.

(35) Zhou, F.; Liu, S.; Pang, Y.; Li, J.; Xin, H. Effects of coal functional groups on adsorption microheat of coal bed methane. *Energy Fuels* **2015**, *29*, 1550−1557.

(36) Yu, S.; Yan-ming, Z.; Wu, L. Macromolecule simulation and CH4 adsorption mechanism of coal vitrinite. *Appl. Surf. Sci.* **2017**, *396*, 291−302.

(37) Jing, B.; Balucan, B.; Underschultz, C.; Pan, D.; Steel, B. Chemical stimulation for enhancing coal seam permeability: Laboratory study into permeability variation and coal structure examination. *Int. J. Coal Geol.* **2020**, *219*, 103375.

(38) Zhang, L.; Kang, T.; Kang, J.; Zhang, X.; Zhang, B.; Chai, Z.; Zhang, R.; Wang, Y.; Kang, G.; Zhao, G. Effect of cyclical microwave modification on the apparent permeability of anthracite: A case study of methane extraction in Sihe mine, China. *ACS omega* **2021**, *6*, 15001−15011.

(39) Su, X.; Wang, Q.; Song, J.; Chen, P.; Yao, S.; Hong, J.; Zhou, F. Experimental study of water blocking damage on coal. *J. Pet. Sci. Eng.* **2017**, *156*, 654−661.

(40) Agi, A.; Junin, R.; Jaafar, M. Z.; Sidek, M. A.; Yakasai, F.; Gbadamosi, A.; Oseh, J. Laboratory evaluation to field application of ultrasound: A state-of-the-art review on the effect of ultrasonication on enhanced oil recovery mechanisms. *J. Ind. Eng. Chem.* **2022**, *110*, 100−119.

https://doi.org/10.1021/acsomega.2c06425
ACS Omega 2023, 8, 1079−1087

(41) Hamida, T.; Babadagli, T. Displacement of oil by different interfacial tension fluids under ultrasonic waves. *Colloids Surf., A* **2008**, *316*, 176−189.
(42) Qin, T.; Javanbakht, G.; Goual, L.; Piri, M.; Towler, B. Microemulsion-enhanced displacement of oil in porous media containing carbonate cements. *Colloids Surf., A* **2017**, *530*, 60−71.

https://doi.org/10.1021/acsomega.2c06425
ACS Omega 2023, 8, 1079−1087